View Article Online / Journal Homepage / Table of Contents for this issue



# Morphology evolution of $GaPO_4$ mesocrystals in a nonionic triblock copolymer system by pH-dependent control†

**Chung-Sung Yang,* Chun-Jung Chen and Xin-Hong Lin**

*Received (in Montpellier, France) 14th November 2006, Accepted 1st December 2006*
*First published as an Advance Article on the web 12th January 2007*
**DOI: 10.1039/b616628h**

In the synthesis of gallium phosphate, $GaPO_4$, crystals *via* a hydrothermal route, using amphiphilic triblock copolymer F127, $[(EO)_{106}(PO)_{70}(EO)_{106}]$–OH, as a surfactant-template, a pH-dependent morphology evolution is observed in the progress of crystal growth. By altering the initial pH level from 7.34 to 11.54, the morphology of crystals is varied from the mesoscale assembly of nanoparticles with porosity, so-called porous mesocrystals, to colloidal crystalline nanoparticles. Thus far, the porous $GaPO_4$ mesocrystals created by self-assembled nanoparticles, is reported for the first time. The typical pore size distribution of porous $GaPO_4$ mesocrystals derived from the adsorption branch by the Barrett–Joyner–Halenda (BJH) model ranges from 1.0 to 3.5 nm with a major distribution peak centered at 2.5 nm.

Published on 12 January 2007 on http://pubs.rsc.org | doi:10.1039/B616628H
Downloaded by University of Belgrade on 01 January 2013

## 1 Introduction

Phosphate-based molecular sieves have been widely applied in the areas of ion exchange, separations and catalysis, by using the phosphate-based chiral tetrahedral configuration in the structure.[1–5] The close connection between the microscopic structure and the macroscopic properties of phosphate-based molecular sieves allows them to recognize, discriminate, and organize molecules with a precision of 1 Å.[5] Nevertheless, since the discovery of mesoporous silica, many efforts have focused on the development of mesoporous silica materials with hierarchical structure, because mesostructured materials (for example MCM-41[6] and SBA-15[7]) may be more versatile for use in separation, catalysis, and sensors than microporous materials.[8] Although, the $MPO_4$ framework is the "3–5" analogue of the "4–4" pure $SiO_2$, to-date no successful synthesis of mesostructure phosphate-based materials has been reported. Generally, it is difficult to synthesize mesoporous materials with crystalline shapes, and especially with uniform morphology, because mesoporous materials synthesized by the cooperative assembly of surfactants, while showing obvious order on the mesoscopic scale show little short-range order on the atomic length scale.[3,9] On the other hand, microporous materials usually exhibit well-defined crystal morphology corresponding to their order at the atomic level.[9] There are only few examples, such as MCM-48 (*Ia*3*d*),[10] with dodecahedral shape, and SBA-1 (*Pm*3*n*)[11] with crystal morphologies of a large number of facets, which successfully demonstrate both mesoporous structure and crystalline property.

Recently, a non-classical crystallization method, denoted as mesocrystal reaction, has been introduced to prepare porous mesoscale crystals.[12] The structure of this type of crystal is created by self-assembled and aligned crystalline nanoparticle building units with the assistance of the structure-directing template. The inter-space between nanoparticles created by surfactant-template is responsible for the porosity existing inside the mesocrystal. This new technology offers us a possibility to rationally design the synthesis of $MPO_4$ crystals with porosity, typically for $GaPO_4$.

The non-ionic triblock copolymer series, $[(EO)_x(PO)_y(EO)_x]$–OH, have been employed in the synthesis and assembly of mesoporous–macroporous silica membranes[13] and in $AlPO_4$ nanowire synthesis.[14] Here, we attempt to synthesize porous $GaPO_4$ crystals using the triblock copolymer F127 $[(EO)_{106}(PO)_{70}(EO)_{106}]$–OH, as a structure-directing agent *via* a hydrothermal route. The hydrothermal synthesis is generally considered as an inexpensive and an environmentally friendly route to produce crystalline materials. The crystal quality obtained from this hydrothermal process meets the requirements for electron microscopy and X-ray diffraction investigations, without requiring further annealing.

## 2 Experimental

### 2.1 Chemicals

Gallium oxide and phosphoric acid were purchased from Aldrich and J.T. Baker, respectively. F127 was obtained from BASF. Doubly de-ionized water was used without any further purification. HPLC grade methanol and reagent grade ethanol were purchased from Aldrich, and used as supplied.

### 2.2 Synthesis and characterization

Triblock copolymer F127 was dissolved completely in de-ionized water, with a mole ratio of F127 : $H_2O$ = 1 : 1000, and retained as a stock solvent. $GaPO_4$ crystals were synthesized *via* the reaction of gallium oxide (1 mmol) and phosphoric acid (0.1 mL) in the stock solvent, with variable initial pH values. The reactants were mixed and well stirred in a 30 mL Teflon-lined stainless steel autoclave. After the addition of a suitable alkaline medium to adjust the pH values,

*Department of Applied Chemistry, National Chia Yi University, Chia Yi, Taiwan 60004, R.O.C.. E-mail: csyang@mail.ncyu.edu.tw; Fax: +886-5-271-7901; Tel: +886-5-271-7962*

† Electronic supplementary information (ESI) available: EDS spectrum for porous $GaPO_4$ crystals. See DOI: 10.1039/b616628h

View Article Online

**Table 1** Reaction conditions and results

| $GaPO_4$ | Initial pH | Final pH | Morphology |
|---|---|---|---|
| GP-1 | 7.34 | 6.97 | White powder (rods (major) + NPs[a]) |
| GP-2 | 8.72 | 7.75 | White powder (rods (major) + NPs) |
| GP-3 | 10.07 | 8.37 | White powder (rods + NPs)[b] |
| GP-4 | 10.68 | 8.72 | White powder (rods + NPs) |
| GP-5 | 11.54 | 9.33 | White powder (NPs) |
| GP-6 | 12.59 | 10.54 | Liquid |
| NGP-1 | 7.44 | 7.12 | White flakes[c] |
| NGP-3 | 10.11 | 9.54 | White flakes |
| NGP-5 | 11.59 | 10.84 | White flakes |

[a] NPs = nanoparticles. In GP-1 and GP-2, rods are the major product. [b] The amount of rod-shaped crystals in GP-3 or GP-4 is lower than that in GP-1 or GP-2. [c] The NGP-X series are products synthesized by the same route as that of the GP-X series, except for the absence of F127.

Published on 12 January 2007 on http://pubs.rsc.org | doi:10.1039/B616628H
Downloaded by University of Belgrade on 01 January 2013

the vessels were sealed, then heated at 180 ± 2 °C for 4 days. White precipitates were obtained from the reactions after removing the supernatant in the vessel, and were washed several times with ethanol–water mixed solvent. The resultant solids are denoted as GP-X (X = experiment series number shown in Table 1). The yield of the samples were about 50–70 wt%. The NGP-X series were products synthesized by the same route as that of the GP-X series, except for the absence of F127.

Powder X-ray diffraction (XRD) was measured on a Shimadzu X6000, at room temperature, using Cu-Kα radiation. Scanning electron microscopy (SEM) images were obtained from a Hitachi S-3500N. Samples were deposited on to conducting carbon film and coated by Au ion sputtering at room temperature. SEM energy dispersive spectroscopy (EDS) was performed with 25 keV voltage. Transmission electron microscope (TEM) micrographs were obtained on a JEOL 2010-HR with 200 keV accelerating voltage. Samples were prepared by evaporation of the colloidal solution on a 200-mesh Cu grid. Fourier-transform infrared (FT-IR) spectra were measured on a Thermo Nicolet Avatar 360 spectrophotometer. The surface areas and pore volumes of $GaPO_4$ rods were recorded from a Brunauer–Emmett–Teller (BET) method by a BELSORP-mini-II. Samples were calcined at 400 °C for 3 h before the BET experiments. All data were collected at room temperature.

## 3 Results

The triblock copolymer F127 $[(EO)_{106}(PO)_{70}(EO)_{106}]$–OH can initiate the nucleation of nanocrystals at room temperature by offering an amphiphilic environment where the nanocrystallites can grow.[13] Meanwhile, the hydrophilic $(EO)_{106}$ fraction of surfactant-template F127 facilitates the mesoscale self-assembly of nanoparticles by van der Waals forces or molecular coordination forces. On the other hand, the hydrophilic $(EO)_{106}$ fraction also provides the required weak intermolecular coordinating force to prevent the agglomeration of nanoparticles, and to create the porosity inside the crystal. Here, the key parameters chosen to study the influence on the crystal evolution of $GaPO_4$ in the F127 system, are the initial pH, and the change in pH during the reaction. The temperature and mole ratios of the reactants are kept constant to enable parameter control. No crystalline materials could be found in the reactions starting from an acidic solution (pH < 7). At highly alkaline levels (pH ≥ 12.5), only a clear solution is found at the end of reaction.

The synthesis conditions, the changes in pH during the reactions, and reaction results obtained for the $GaPO_4$ syntheses are listed in Table 1. The final products were dried, and stored as powders, or suspended in methanol–ethanol for further study. The morphology and quality of the crystallites varied with the initial pH of reaction. GP-1, GP-3 and GP-5 were selected to evaluate the crystal evolution during the reaction progress. These $GaPO_4$ crystals are stable for several months in a methanol–ethanol solution, without any change of morphology or color.

### 3.1 GP-1

**3.1.1 Characterization by SEM, XRD and TEM.** GP-1 was prepared by a hydrothermal synthesis with initial pH = 7.34. The final product is white needle-shaped crystals as observed by optical microscopy. The pH at the end point of the 96 h reaction drops to almost neutral, pH = 6.97. A typical scanning electron microscopy (SEM) image for the as-prepared GP-1 crystals, Fig. 1(a), shows a large numbers of crystalline rods. The diameters of these rods mostly range from 2 to 5 μm with an average aspect ratio (length/diameter, $L/D$) > 15. The qualitative microanalysis of elements was carried out by energy dispersive spectra (EDS) of SEM. The EDS spectra confirms the existence of Ga ($L_{\alpha 1}$ = 1.104 eV and $K_{\alpha 1}$ = 9.241 eV) and P ($K_{\alpha 1}$ = 9.241 eV) in the rod-shaped crystals.[15] The powder X-ray diffraction (XRD) pattern (Fig. 1(b)) for GP-1 is consistent with a mixed structure of cubic and orthorhombic phases of $GaPO_4$.[16] The formation of a mixed phase in GP-1 is due to the nucleation and aggregation of crystallites into rods being highly sensitive to environmental factors.[14,17,18] The average size for GP-1 samples, derived from the orthorhombic (201) peak by the Scherrer equation, is about 8.8 nm (diameter) that is far from the data (2–5 μm) directly measured from SEM images. The large difference in the diameter data obtained from the XRD pattern and the SEM image suggests that the rod-shaped GP-1 is likely to be composed of secondary structures, such as nanocrystallites. In general, the secondary nano-crystallite structure in an inorganic crystallization process usually fuses to a single crystal in order to reduce the lattice energy.[12,19] A small-angle ($2\theta$ = 1.0–4.0°) X-ray diffraction spectrum (SAXS) for GP-1 was measured to further investigate the secondary structure of GP-1. From the diffraction pattern, Fig. 1(c), two well-defined peaks are observed and are indexed

 This journal is © the Royal Society of Chemistry and the Centre National de la Recherche Scientifique 2007

Published on 12 January 2007 on http://pubs.rsc.org | doi:10.1039/B616628H
Downloaded by University of Belgrade on 01 January 2013

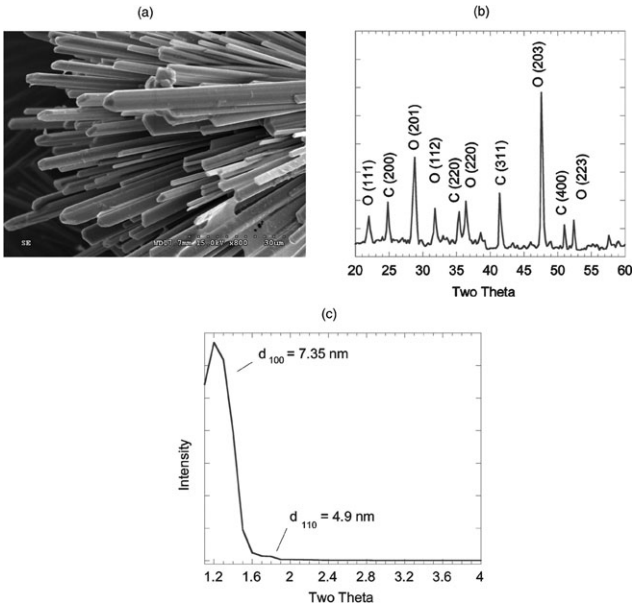


**Fig. 1** (a) A SEM image for the as-prepared GP-1 crystals. The length of the GP-1 is about several tens of μm with aspect >15. (b) Powder XRD for GP-1. The pattern shows a mixed structure of cubic and orthorhombic phases (GCPDS 31-0547 and 31-0546). The diameter for GP-1, derived from orthorhombic (201) peak is about 8.8 nm, (c) A small-angle XRD pattern for GP-1. Two well-defined peaks at $d$ = 73.5 Å ($d_{100}$) and $d$ = 49 Å ($d_{110}$) are observed.

to $d_{100}$ (7.35 nm) and $d_{110}$ (4.9 nm) of the face centered cubic ($F\bar{4}3m$) space group. These two diffraction peaks are attributed to the lowered symmetry of the crystal or different orientations of the mesophase domains.[9] The SAXS confirms that GP-1 is a crystal assembled by different orientation of mesophase domains, *i.e.* a crystal created by individual domains (nanoparticles) with mesoscale transformation or assembly, so called mesocrystals.[12,19]

Transmission electron microscopy (TEM) and high-resolution TEM (HR-TEM) are used to establish and to confirm the identity of the GP-1 rods isolated from methanol–ethanol solution. A TEM micrograph for a single strand of GP-1 is provided in Fig. 2(a), and a close-up image of the marked area in Fig. 2(a) is shown in Fig. 2(b). From the TEM images, it is clearly observed that a large number of nanoparticles are assembled together to from the facet of the rod. Most of the nanoparticles shown in the image have spherical shapes, and only a few are hexagonal or polygonal. The inter-space between nanoparticles is discernable, (>1 nm) and the overlapping between nanoparticles is not evident in the image. The size distribution of these nanoparticles mainly ranges from 7 to 12 nm (diameter), which is consistent with the diameter data derived from the powder XRD, Fig. 1(c). The observed morphology from TEM images clearly reveals that the crystallization of GP-1 employs self-assembly of colloidal nanoparticles and mesoscale transformation to create rod-shaped crystal crystals, and the discernable inter-spaces between nanoparticles is indicative of porosity inside the GP-1 crystals.[12,19]

**3.1.2 Porosity measurement.** The nitrogen sorption isotherms of GP-1 rods (calcined at 400 °C for 3 h) yields a type

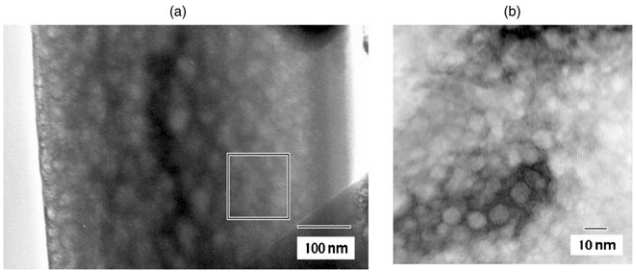


**Fig. 2** (a) A TEM micrograph for a single strand of the GP-1 product. In this image, the surface of the GP-1 is not smooth. (b) A blow up of the marked area shown in (a). The spaces between nanoparticles is discernable and the overlapping between nanoparticles is not evident in the image. The diameter of these nanoparticles mostly varied from 7 to 12 nm.

H3 hysteresis loop,[20] as shown in Fig. 3. Hysteresis is usually associated with capillary condensation in mesoporous structures and the type H3 hysteresis loop is observed with aggregates of particles giving rise to slit-shaped pores.[20] The surface areas and pore volumes of GP-1 rods are obtained from the Brunauer–Emmett–Teller (BET) method. The average surface area is 37.11 $m^2\ g^{-1}$ and pore volume = 60.32 $mm^3\ g^{-1}$ for GP-1 rods. The precise pore size data are measured from the adsorption branch by the Barrett–Joyner–Halenda (BJH) model. A pore size distribution derived from the BJH curve is provided in the inset of Fig. 3. The pore-size distribution peak is centered at 2.5 nm. These results show that the rod-shaped GP-1 crystals are in a meso-structured material with a pore size distribution between 1.0 and 3.5 nm. The investigation for the creation of meso-porosity in the $GaPO_4$ rods synthesized from the F127 environment is still ongoing. However, there is no doubt that the porosity should be related to the nature of triblock copolymers F127 and the pH level in the reaction.[14]

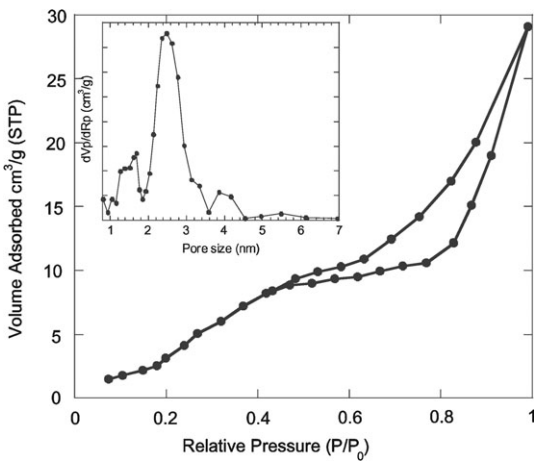


**Fig. 3** The nitrogen sorption isotherms of GP-1 yields a type H3 hysteresis loop. The average surface area is 37.11 $m^2\ g^{-1}$ and pore volume = 60.32 $mm^3\ g^{-1}$ for GP-1 rods. The pore size distribution is shown in the Barrett–Joyner–Halenda (BJH) curve, inset of Fig. 3. The pore-size distribution peak is centered at 2.5 nm.

Published on 12 January 2007 on http://pubs.rsc.org | doi:10.1039/B616628H
Downloaded by University of Belgrade on 01 January 2013

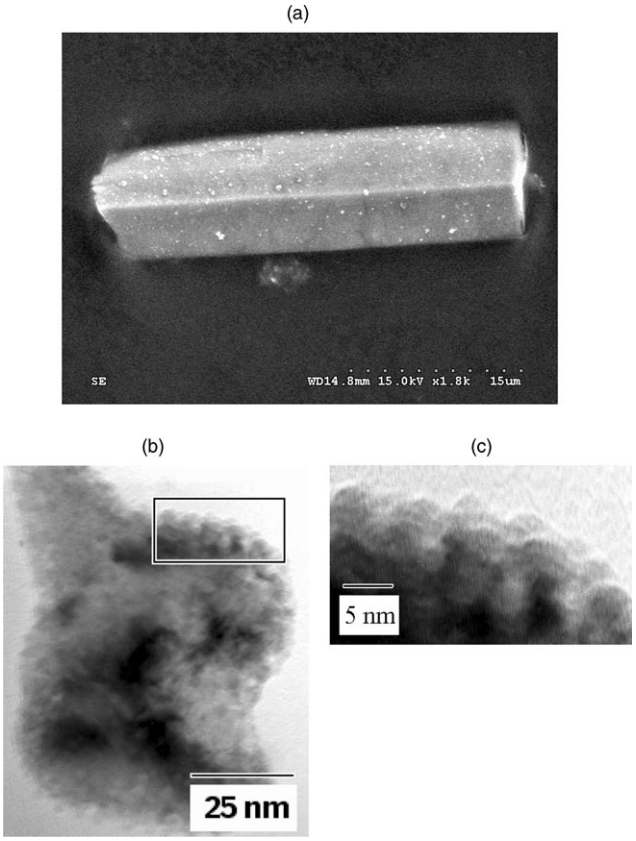


**Fig. 4** (a) A typical SEM image for the GP-3 product, synthesized from an initial pH = 10.07 reaction. The diameters of GP-3 range from 2 to 4 μm ($3 < L/D < 10$). (b) A TEM micrograph for a fraction of the GP-3 sample. The architecture of the fraction of the GP-3 rod shows a mesoscale assembly of nanoparticles. (c) The inter-space of the assembled nanoparticles is clearly discernible. No obvious overlapping between nanoparticles is evident. The diameter of the nanoparticles of GP-3 is in the range of 3–8 nm.

## 3.2 GP-3

**3.2.1 Characterization by SEM, XRD and TEM.** A typical SEM image for the GP-3 sample, synthesized from a 96 h reaction with an initial pH = 10.07, is shown in Fig. 4(a). The morphology of the sample is of short rectangular rods. The diameters of the GP-3 rods range from 2 to 4 μm ($3 < L/D < 10$). In comparison with GP-1, the size of GP-3 is obviously smaller in both length and diameter. The yield of GP-3 (~49.5 wt%) is about 20% lower than that of GP-1 (~70 wt%). The growth rate of $GaPO_4$ crystallites in a stronger alkaline medium (initial pH = 10.03) is less-directed by the solvent–inorganic interface interaction than that for a weakly alkaline medium (initial pH = 7.80).[14,21] In addition, the solubility of GP-3 is expected to increase by a directed solvent–inorganic interface interaction,[21] which makes GP-3 particles smaller than GP-1 particles in both diameter and length. In the high-vacuum procedure of TEM sampling, the rectangular shape of GP-3 is decomposed. The high-resolution TEM micrograph for a small fraction of GP-3 rods, Fig. 4(b), shows the architecture of the product is similar to GP-1. In Fig. 4(c), the blow-up image for the marked area in Fig. 4(b), the topology of the product is an assembly of aligned nanoparticles building units to develop the external faces that resemble facets of a single crystal.[19] The size distribution of the nanoparticles in GP-3 ranges from 3 to 8 nm, as directly measured from TEM images, which is similar to the sizes of the nanoparticles assembled in the GP-1 architecture. The powder XRD of GP-3 matches the mixed-structure of cubic and orthorhombic phases of $GaPO_4$ and the SAXS of GP-3 is almost identical to that of GP-1. Both the TEM and XRD data support the structure of GP-3 as being the same as GP-1 *i.e.* a meso-structured crystal.

**3.2.2 Characterization by FT-IR and porosity measurement.** Fourier-transform infrared (FT-IR) spectroscopy is used to identify and to characterize the external faces condition of the GP-3 samples. In Fig. 5, four characteristic modes are shown at 2960, 2926, 1423 and 1252 $cm^{-1}$. The band assignments to the functional groups are taken from literature.[22] The peaks located at 2960 and 2926 $cm^{-1}$ are assigned to the asymmetric and symmetric stretching of terminal $–CH_3$ groups in $(PO)_{70}$ fractions.[22] The peak at 1423 $cm^{-1}$ is $–CH_2–$ scissoring and the peak at 1252 $cm^{-1}$ corresponds to the saturated aliphatic C–O–C asymmetric stretching.[22] These peaks arise from either the $(EO)_{106}$ or $(PO)_{70}$ fraction.[14] The data confirm the presence of structure-directing polymers F127 either on the external faces of nanoparticles or in the interior between aligned nanoparticles of meso-structured GP-3 crystals.

The nitrogen sorption isotherm of GP-3 rods (calcined at 400 °C for 3 h) is almost identical to that of GP-1, a type H3 hysteresis loop. This result is in accord with the structure observed by XRD and TEM images of porous mesostructured crystals assembled by the aggregates of nanoparticles. The average surface area of GP-3 is 35.61 $m^2\ g^{-1}$ and pore volume = 62.32 $mm^3\ g^{-1}$. The pore-size distribution peak is centered at 2.3 nm.

On the basis of the GP-3 characterization data, the mesoscale transformation of the colloidal nanoparticle to form meso-structured crystals is possibly controlled by the mechanism that brings the nanoparticles together, through gel phase diffusion, by dehydration and polymerization of the hydrophilic $(EO)_{106}$ domains of F127.[23,24] A detailed mechanism is discussed in the following paragraph.

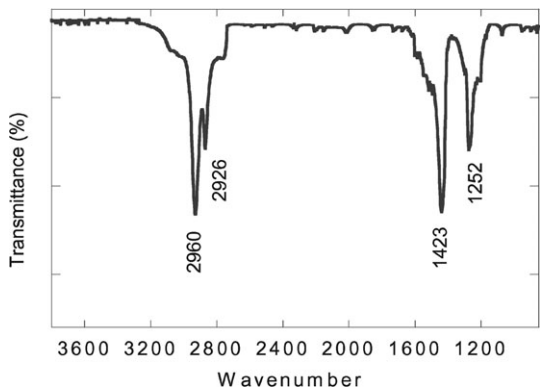


**Fig. 5** The FT-IR spectrum of GP-3 showing four characteristic modes at 2960, 2926, 1423 and 1252 $cm^{-1}$.

 This journal is © the Royal Society of Chemistry and the Centre National de la Recherche Scientifique 2007

Published on 12 January 2007 on http://pubs.rsc.org | doi:10.1039/B616628H
Downloaded by University of Belgrade on 01 January 2013

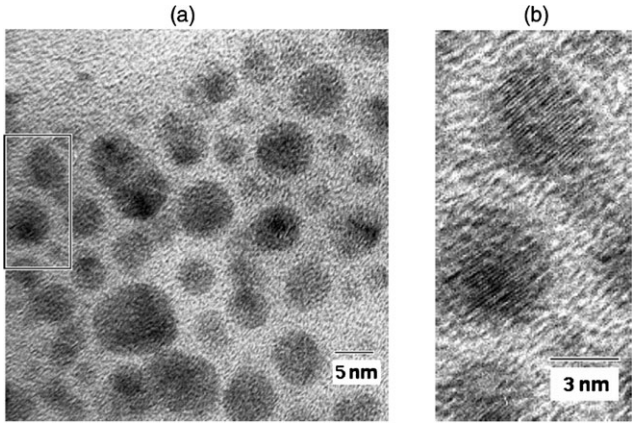


**Fig. 6** (a) A TEM image for GP-5, a reaction with an initial pH = 11.54. A large amount of colloidal nanoparticles was formed. The diameter of $GaPO_4$ nanoparticles in the images ranges from 5–15 nm. (b) The *d*-spacing of the lattice (1.75 Å) of GP-5 nanoparticles matches the (400) phase of cubic $GaPO_4$ (JCPDS-31-0547).

### 3.3 GP-5

**3.3.1 Characterization by TEM and FT-IR.** Fig. 6(a) shows a TEM image for GP-5, a reaction with an initial pH = 11.54, which illustrates a large amount of colloidal crystalline nanoparticles. The diameters of GaP-5 nanoparticles in the images mainly lie in the range 5–15 nm. The *d*-spacing of the lattice (1.75 Å) directly measured from Fig. 6(b) matches the (400) phase of cubic $GaPO_4$. The yield of the GP-5 sample is about 70 wt%. If the initial pH level is raised to 12.5 or higher, the final product is a clear liquid with no precipitate. Since the reaction parameters, such as temperature, molar ratio of reactants, concentration of surfactant-template, and reaction time are carefully controlled, the morphology variation from meso-structured crystal (GP-1, GP-3) to colloidal nanoparticles (GP-5) would be introduced by the differences in pH levels of the initial and end points among GP-1, GP-3 and GP-5.

The IR spectrum of GP-5 is shown in Fig. 7. Five characteristic modes, *i.e.* 3345, 2962, 2920, 1427, and 1246 $cm^{-1}$, are observed. The IR spectrum of GP-5 is similar to that of GP-3, except for the new peak at 3345 $cm^{-1}$. The peak of 3345 $cm^{-1}$ is attributed to the free O–H mode of $(EO)_{106}$ fractions,[14,22] confirming the presence of the terminal OH group of F127, $(EO)_{106}(PO)_{70}(EO)_{106}$–OH, and giving evidence to prove the dehydration reaction does not propagate in the GP-5 reaction.[14] At the pH = 11.54 reaction, the process of transformation from colloidal nanoparticles to mesocrystals does not occur because the end-point pH is too high (= 9.33). The thermodynamic driving force (dehydration reaction) toward compact crystal formation is interrupted by the free $[OH]^-$ ions because a reverse reaction (hydration reaction) will take place.[14] The evidence for this is that the terminal OH group of F127 still can be measured by IR spectra for GP-5 samples. The mesocrystals exist as a short-lived intermediate in the solution and finally decompose back into colloidal nanoparticles.[12,19] From these results, it is clear that the formation of mesostructured crystals obviously relies on the concentration of unconsumed free $[OH]^-$ ions.

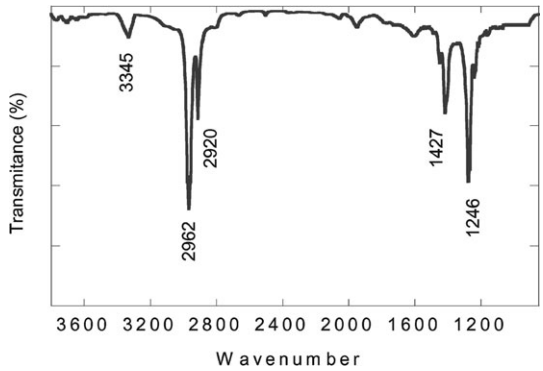


**Fig. 7** In the FT-IR spectrum of GP-5, five characteristic modes are shown: 3345, 2962, 2920, 1427 and 1246 $cm^{-1}$. These five peaks confirm the presence of F127 triblock copolymers on the surface of GP-5.

### 3.4 NGP-X

The habit and morphology of NGP-1, NGP-3 and NGP-5 are provided in Table 1. The changes in pH between the initial and end points for NGP-1, NGP-3 and NGP-5 are much smaller than those for GP-1, GP-3 and GP-5, respectively. In the SEM micrograph of the NGP-1 products, no evidence of nanoparticles, or mesocrystals could be found, but a number of irregular polygonal chunky flakes ($>1$ $\mu m^3$) are observed. Similar results can be seen in the SEM images for NGP-3 and NGP-5, which reveal that the formation and evolution of morphology for $GaPO_4$ mesocrystals is not only pH dependent but is also affected by the participation of surfactant-template F127.

## 4 Discussion

During the synthesis processes of $GaPO_4$ crystals, we learn that pH is a main parameter in determining the structure of final products, in addition to the structure-directing agent, F127. The states of condensation of metalate ions obtained by hydrolysis of a metal salt are controlled by the pH of the medium.[24] Close monitoring of pH variations, *i.e.* the concentration of $[OH^-]$, during the progression of the hydrothermal reaction is necessary to investigate the formation mechanism of porous $GaPO_4$ mesocrystals. Based on this understanding, we propose a pH-dependent model to describe the $GaPO_4$ crystal evolution from porous rod-shaped mesocrystal to crystalline nanoparticles in the F127 system. A detailed mechanism is provided in Scheme 1.

In a water-rich F127–water binary system, F127 copolymers were dissolved in water as individual molecules at room temperature. The equilibrium of the triblock copolymer system will change after the addition of inorganic precursors and a new competition among all species, including monomers, will be triggered until a new equilibrium is reached.[25] As the temperature rises and the concentration of copolymer monomers reaches the critical micelle concentration (cmc), F127 monomers are self-assembled in an aqueous phase as many amphiphilic domains, step 1-(a) in Scheme 1.[14,25,26] The hydrophilic $(EO)_{106}$ domains intrude into the aqueous phase

Published on 12 January 2007 on http://pubs.rsc.org | doi:10.1039/B616628H
Downloaded by University of Belgrade on 01 January 2013

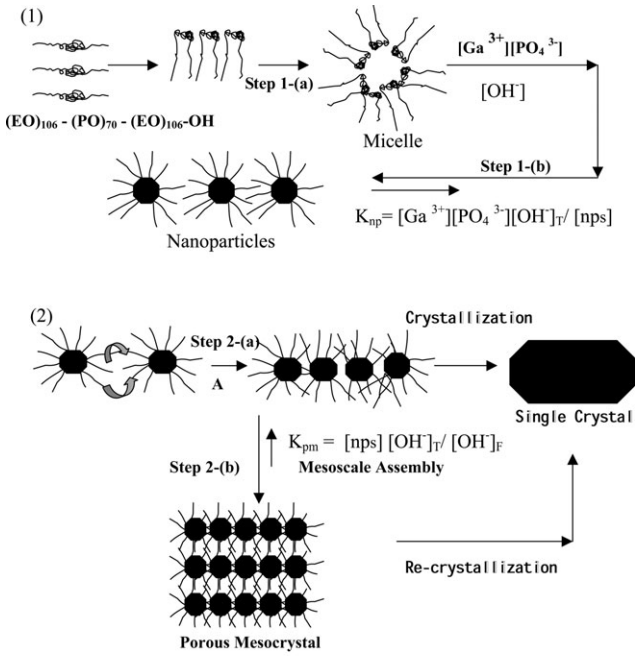


**A: dehydration of two $(EO)_{108}$ fractions under basic condition.**

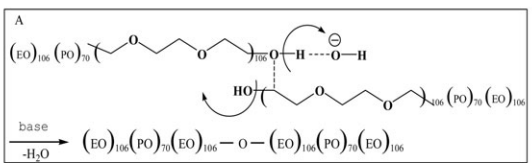


**Scheme 1** Morphology evolution of porous $GaPO_4$ mesocrystal.

and hydrophobic $(PO)_{70}$ domains occupy the inner sphere of the micelle.[25,26] The active nucleophilic sites (O-sites) of $(PO)_{70}$ fractions can easily chelate $Ga^{3+}$ ions inside the hydrophobic domains, while the $(EO)_{106}$ fractions show a weak intermolecular coordinating force to segregate from other micelles.[23,26] The interaction between gallium cations and hydroxide anions is strong enough to transport $Ga^{3+}$ cations from the aqueous phase into the hydrophobic $(PO)_{70}$ fraction of the micelle core, but not strong enough to prevent $Ga^{3+}$ cations from reacting further to create the desired building units, *i.e.* nanoparticles, step 1-(b) in Scheme 1. These nanoparticles were then allowed to grow in a confined amphiphilic environment.[23] Meanwhile, the alkaline environment also favored the ionization of phosphoric acid to dihydrogen phosphate ion, and finally to hydrogen phosphate ion and its conjugate base, $PO_4^{3-}$. The ionization of phosphoric acid to $PO_4^{3-}$ was maximized above pH = 7, and $GaPO_4$ nanocrystallites grew appreciably in such an alkaline environment.[14,27] The formation constant of nanoparticles is favored by $[Ga^{3+}][PO_4^{3-}]$ and the total concentration of $[OH^-]$, denoted as $[OH^-]_T$. All $GaPO_4$ nanocrystallites, in this step, grow at the expense of a decrease in pH. After consumption of all available $Ga^{3+}$ and most free $OH^-$ ions, the nucleation of $GaPO_4$ nanocrystallites stopped and the end point pH level dropped 1–2 pH unit(s).

The process of condensation of spherical nanoparticles then takes place. The unconsumed free $OH^-$ ions, $[OH^-]_F$, initiated the dehydration condensation between the hydrophilic $(EO)_{106}$ fraction, step 2-(a) in Scheme 1:[25,26]

$$(EO)_{106}(PO)_{70}(EO)_{106}\text{–OH} + \text{HO–}(EO)_{106}(PO)_{70}(EO)_{106} \rightarrow (EO)_{106}(PO)_{70}(EO)_{106}\text{–O–}(EO)_{106}(PO)_{70}(EO)_{106} + H_2O$$

The dehydration and polymerization between $(EO)_{106}$ domains is rapidly initiated, due to the proximity of the hydrophilic $(EO)_{106}$ fractions, but turns to a slow step because of the substantial depletion of most available free $OH^-$ ions during the reaction.[25,26] The dehydration condensation helps to decrease the thermodynamic entropy, which occurs either by a rise in temperature or by the free motion of molecules.[25,26] In the previous paragraph, we mentioned that the $(EO)_{106}$ fractions had a weak intermolecular coordinating force to segregate from other micelles. This intermolecular coordinating force creates the inter-space between two nanoparticles. The inter-space size between two nanoparticle domains, *i.e.* pore size, depends on the situation of interaction between $(EO)_{106}$ fractions. On the basis of the pore diameter distribution peak obtained from the BJH model, the pore sizes of the inter-space in this case range from *ca.* 1.0 to 3.5 nm.

When the reaction was allowed to start at higher initial pH levels (pH = 10.07 for GP-3, 10.68 for GP-4, and pH = 12.54 for GP-5), the sizes of rod-shape crystals decreased in both diameter and length. The reason is that the free $OH^-$ ions not only influence nucleation through transport of $Ga^{3+}$ from the aqueous phase into the hydrophobic $(PO)_{70}$ domain, but also control the crystal growth by condensation of $Ga^{3+}$ into crystallites. In the GP-3 and GP-4 conditions, the numbers of available free $OH^-$ ions were much higher than those in GP-1 and GP-2 (pH = 7.34 and 8.72, respectively). The starting reagent $Ga_2O_3$ was quickly dissolved into the aqueous solution as $Ga^{3+}$ ions and the remaining free $OH^-$ ions conjugated with water molecules rapidly transported these $Ga^{3+}$ into micelles. The nucleation speed of nanocrystallites is obviously enhanced and the evolution numbers of nanocrystallites increased spontaneously by the sufficient supply of $Ga^{3+}$. The dehydration condensation between $(EO)_{106}$ domains continued, but the reverse reaction, decomposition of the rod-shape $GaPO_4$ mesocrystals into colloidal nanoparticles, was boosted by the strong alkaline environment. In the final step, step 2-(b) in Scheme 1, the mesoscale assembly of nanoparticles was no longer possible and the meso-structured crystal was decomposed back into colloidal nanoparticles, *i.e.* GP-5. From this result, we found that the formation constant of porous $GaPO_4$ mesocrystals was not directly related with the concentration of $[OH^-]_T$ used in the synthesis, but was affected by $[OH^-]_F$ in the solution.[14]

At highly alkaline levels, (pH > 12.54), the reactant $Ga_2O_3$ was completely dissolved into solution at expense of $[OH]^-$ ions and the pH value decreased quickly to 10.54. In such a strong alkaline medium, all possible products were dissolved into solution, and a clear solution without any precipitation was obtained at the end of reaction.

## 5 Conclusion

Porous $GaPO_4$ rod-shaped mesocrystals are synthesized by means of inorganic reagents in the amphiphilic triblock

 This journal is © the Royal Society of Chemistry and the Centre National de la Recherche Scientifique 2007

copolymer F127 system *via* a hydrothermal reaction under pH-dependent control. In addition to the starting pH level of reactions, the triblock copolymer F127 also plays an essential factor in the creation of the porosity inside the $GaPO_4$ mesocrystals. Therefore, there is no doubt that the triblock copolymer F127 appears to fulfill a critical templating and structure-directing role in the synthesis of the novel porous meso-structured crystals. The generation of a suitable environment for the surfactant-template to mediate the evolution of crystals is responsible for the successful synthesis of porous $GaPO_4$ mesocrystals.

## Acknowledgements

The authors are grateful for the financial support from the National Science Council, Taiwan (NSC 94-2113-M-415-006). Ms Pi-Hua Su's valuable assistance in SEM and EDS is also highly appreciated.

## References

1 S. T. Wilson, B. M. Lok, C. A. Messina, T. R. Cannan and E. M. Flanigen, *J. Am. Chem. Soc.*, 1982, **104**, 1146.
2 P. Feng, X. Bu and G. D. Stucky, *Nature*, 1997, **388**, 735.
3 X. Bu, P. Feng and G. D. Stucky, *Science*, 1997, **278**, 2080.
4 P. Feng, X. Bu and C.-S. Yang, *Microporous Mesoporous Mater.*, 2001, **50**, 145.
5 M. E. Davis and R. F. Lobo, *Chem. Mater.*, 1992, **4**, 756.
6 C. T. Kresge, M. E. Leonowicz, W. J. Roth, J. C. Vartuli and J. S. Beck, *Nature*, 1992, **359**, 710.
7 D. Margolese, J. A. Melero, S. C. Christiansen, B. F. Chmelka and G. D. Stucky, *Chem. Mater.*, 2000, **12**, 2448.
8 M. E. Davis, *Nature*, 2002, **417**, 813.
9 C. Yu, B. Tian, J. Fan, G. D. Stucky and D. Zhao, *J. Am. Chem. Soc.*, 2002, **124**, 4556.
10 J. M. Kim, S. K. Kim and R. Ryoo, *Chem. Commun.*, 1998 259.
11 S. Guan, S. Inagaki, T. Ohsuna and O. Terasaki, *J. Am. Chem. Soc.*, 2000, **122**, 5660.
12 (*a*) T. Wang, H. Colfen and M. Antoietti, *J. Am. Chem. Soc.*, 2005, **127**, 3246; (*b*) H. Colfen and M. Antonietti, *Angew. Chem., Int. Ed.*, 2005, **44**, 5576.
13 C. Yu, B. Tian, J. Fan, G. D. Stucky and D. Zhao, *Chem. Commun.*, 2001, 2726.
14 C.-S. Yang and K.-Y. Kau, *J. Chin. Chem. Soc.*, 2005, **52**, 65.
15 The EDS spectra for $GaPO_4$ is provided in the ESI†.
16 JCPDS 31-0547 and JCPDS 31-0546.
17 C.-S. Yang, M.-S. Shih and F.-Y. Chang, *New J. Chem.*, 2006, **30**, 729.
18 X. Peng, L. Manna, W. Yang, J. Wickham, E. Scher, A. Kadavanich and A. P. Alivisatos, *Nature*, 2000, **404**, 59.
19 Y. Ma, H. Colfen and M. Antonietti, *J. Phys. Chem. B*, 2006, **110**, 10828.
20 K. S. W. Sing, D. H. Everett, R. A. W. Haul, L. Moscou, R. A. Pierotti, J. Rouquerol and T. Siemieniewska, *Pure Appl. Chem.*, 1985, **57**, 603.
21 J. W. Mullin, *Crystallization*, Butterworth–Heinemann, Oxford, UK and Boston, MA, 3rd edn, 1997.
22 G. Socrates, *Infrared Characteristic Group Frequencies*, Wiley, New York and London, 1980.
23 C. Guo, J. Wang, H.-Z. Liu and J.-Y. Chen, *Langmuir*, 1999, **15**, 2703.
24 R. A. Caruso and M. Antonietti, *Chem. Mater.*, 2001, **13** 3272.
25 (*a*) C. Oliver, H. Caldararu and A. Caragheorgheopol, *Langmuir*, 1999, **15**, 1891; (*b*) R. Nagarajan, *Colloids Surf., B*, 1999, **16**, 55.
26 Z. Yang and R. Sharma, *Langmuir*, 2001, **17**, 6254.
27 D. D. Macdonald, P. Butler and D. Owen, *J. Phys. Chem.*, 1973, **77**, 2474.

Published on 12 January 2007 on http://pubs.rsc.org | doi:10.1039/B616628H
Downloaded by University of Belgrade on 01 January 2013